International Conference on Space Optics—ICSO 2022

Dubrovnik, Croatia

3–7 October 2022

Edited by Kyriaki Minoglou, Nikos Karafolas, and Bruno Cugny,

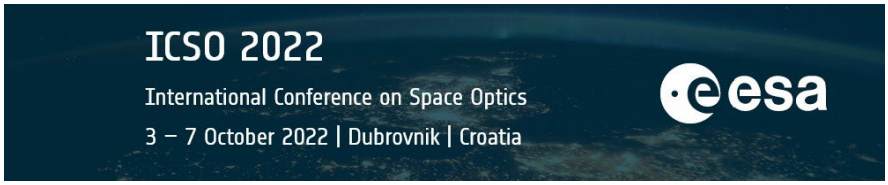

Study and proof of concept of a freeform TMA designed for nanosat space infrared imaging applications

International Conference on Space Optics — ICSO 2022, edited by Kyriaki Minoglou, Nikos Karafolas, Bruno Cugny, Proc. of SPIE Vol. 12777, 1277773 · © 2023 ESA and CNES · 0277-786X · doi: 10.1117/12.2691377

Study and proof of concept of a freeform TMA designed for nanosat space infrared imaging applications

Clément Freslier[1], Guillaume Druart[1], Jean-Baptiste Volatier[1], Thierry Lépine[2], Arnaud Helière[3], Christophe Buisset[3], Tibor Agocs[3]

[1] *ONERA-The French Aerospace Lab, 8 Chemin de la Hunière, 91123 Palaiseau CEDEX, France*
[2] *Univ Lyon, Laboratoire Hubert Curien, CNRS UMR 5516, 41000 Saint-Etienne, France*
[3] *European Space Agency, ESTEC, Keplerlaan 1, 2202 AG Noordwijk, The Netherlands*
clement.freslier@onera.fr

ABSTRACT

Freeform surfaces are a revolution in the field of spatial imaging because they allow the correction of optical aberrations in off-axis systems. Freeform surfaces are defined as non-rotationally symmetric surfaces, which also cannot be described as an off-axis part of a conicoid. The use of such surfaces can also enable to increase performances, such as the field of view, F-number or compactness of off-axis, fully reflective telescopes, and is thus interesting for nanosatellite imaging applications.

In this paper, we will present a proof of concept for a fast, compact and well-corrected freeform Three Mirror Anastigmat (TMA) design suited for nanosatellite infrared thermal imaging using an uncooled micro-bolometer. The performance and tolerance analysis will be presented, along with an analysis of the mirrors' shape and surface quality using an industrial surface characterisation tool. The consequences of the mirrors' shape error on the optical quality will also be discussed, as well as a method to compensate for the loss in image quality induced by these shape defects.

Keywords: Freeform, optical design, nanosatellite, TMA, infrared imaging, shape error

1. INTRODUCTION

In this article, we present a freeform TMA with a rectangular field of view (FOV) for nanosatellite infrared thermal imaging, such as the study of the Urban Heat Island phenomenon.

In urban areas, the concentration of human activity, energy consumed and use of low-albedo and high volumetric heat capacity materials create local areas significantly warmer than the surrounding rural areas. This phenomenon is called Urban Heat Island (UHI). The additional energy used to cool down buildings also adds up to this problem.[1] Those effects can be measured using on-site data as well as remote data collection of the temperature; however, remote measurements allow for finer spatial sampling than using on-site data. To that end, using a constellation of satellites in Low Earth Orbit could also enable shorter revisit times than satellites places in sun-synchronous orbits, and thus a better sample of the circadian cycle.

However, these constellations require that the cost of each individual satellite be low, and with a low mass. Therefore, using CubeSats becomes interesting, as their mass production can be achieved at a reasonable price. Although, it implies manufacturing very compact optical payloads, that can fit in a few cubic decimetres, which only becomes possible using freeform optics. Nonetheless, the manufacturing of freeform optics is a delicate process, although becoming better controlled [2], and can result in form errors that alter the resulting image quality of the system.

2. FREEFORM SURFACES

Designing freeform surfaces implies to handle a high number of parameters, and to implement precise ray-tracing algorithms. However, recent progress made in computing power and new algorithms allows to design and optimise optical systems using such surfaces, and the development of innovative manufacturing techniques makes these concepts realisable.

In a more classical approach, on-axis reflective designs with rotationally symmetric surfaces are admittedly easier to design and manufacture, but they suffer from central obscuration scaling with FOV, and are thus better suited for long-focal, small FOV systems. In order to cope with this issue, off-axis systems using rotationally symmetric systems were designed, although these systems kept relatively small FOV, because of additional asymmetric geometrical aberrations increasing with the de-centring and tilting of the optical surfaces.

Using freeform surfaces allows for a better compensation of those aberrations, and thus enable to achieve designs with larger FOV or F-number. They also allow for compact systems that are better corrected than their classical versions[3]. In addition, fully reflective designs have the advantage of being lightweight, achromatic and potentially manufacturable at a lower cost than catoptric designs due to the use of cheaper materials, which could result in large-scale production of compact panchromatic systems for various applications in visible or infrared spectrum.

Freeform surfaces are most commonly defined as a standard conic surface with corrective term based on 2D polynomials, usually over polar coordinates [4]. However, many other descriptions exist, such as NURBS or radial basis functions [5]. An overview of standard definitions of freeform surfaces definitions is given in Article [6].

In this article, we will focus on two well-established descriptions using either the XY polynomial basis or the normalised Zernike polynomials basis, as these are the ones used during the optical design of the system. The use of the normalised Zernike basis is the most commonly used because it is orthogonal over the unit disc, and thus enables to have a unique decomposition of the surface sag on this basis. This base should be used to describe aberrations of optical systems with circular surfaces, and it can be useful to compare wavefront and surface shape in the same basis.

However, to avoid degeneracy, it is possible to manage the path of the parabasal ray so that it hits the centre of each mirror, requiring that there are no local slope at the surface centre. During the optimisation, the tip and tilt variables must then be computed after each modification of the other variables. However, in orthogonal bases, a local slope at the surface centre is generated by the radial term. To that end, the use of XY polynomials, which do not add a local slope, is favourable, and can speed up the optimisation process in its early stages.

The equation giving the surface sag in the Fringe ordering of the Zernike polynomial basis as a function of radial distance and azimuthal angle is given below:

$$z_{Zernike}(r,\varphi) = \frac{cr^2}{1+\sqrt{1-(1+k)c^2r^2}} + \sum_{i=1}^{N} A_i Z_i(\rho,\varphi) \quad (1)$$

In this description, c is the curvature of the surface, k is the conic constant and Z_i is the i-th Zernike polynomial, itself a function of the normalised radius $\rho = \frac{r}{r_{pupil}}$ and azimuthal angle φ.

For the XY polynomials, the surface description uses Cartesian coordinates:

$$z_{XY}(x,y) = \frac{cr^2}{1+\sqrt{1-(1+k)c^2r^2}} + \sum_{k=0}^{N} A_k x^i y^j \ \ where\ i+j \leq k \quad (2)$$

Every surface can then be described by more coefficients than the radius and conic constant, used to represent conic surfaces. The added complexity is overcome thanks to the improvements in computational power that modern computers offer.

3. SYSTEM SPECIFICATIONS AND OPTICAL DESIGN

3.1 Specifications

In this section, we give the main requirements driving the design of the optical payload:

1. The payload must provide images in the thermal infrared spectrum with several spectral bands in order to be able to correct atmospheric and emissivity effects and retrieve the Land Surface Temperature. A central wavelength of $10\ \mu m$ was chosen for this system.
2. The Ground Spatial Resolution (GSD) must be between 50 and$100m$, with a 50 to $100km$ swath.
3. The volume allocated to the optical payload is $100x200x300\ mm^3$, corresponding to a 6U CubeSat in Low Earth Orbit.

We chose to study an off-axis unobscured telescope with an uncooled microbolometer [5]. The mirrors are made of aluminium so that the system can be athermalized by using the same material for the mechanical structure.

The use of an uncooled detector requires a low F-number, below 1.5, to ensure an acceptable Noise Equivalent Temperature Detection (NETD). The NETD is defined as the smallest temperature variation that induces a signal change equal to the noise, i.e. a SNR of 1.

The spatial resolution of the instrument is limited by the pixel size, whose instantaneous Field of View (IFOV) depends on the focal length of the instrument. Knowing the altitude of the spacecraft, the IFOV can be expressed as a function of the GSD. For this design, we chose a $70m$ GSD, compliant with the requirements, and the altitude has been calculated to be around $570km$. The pixel size of our detector is $12\mu m$. The required focal length can then be deduced:

$$f = \frac{spacecraft\ altitude * pixel\ size}{GSD} \approx 100mm \tag{3}$$

The half FOV along each direction is given by

$$half\ FOV = tan^{-1}\left(\frac{half\ image\ size}{f}\right) \tag{4}$$

Thus,

$$half\ FOV_X \approx 2.20\ °$$

$$half\ FOV_Y \approx 1.65°$$

Furthermore, to take into account the mirrors substrate, the mechanical design and the detector electronics, a $100 \times 150 \times 250\ mm^3$ will be allocated to the optical design itself. Table 1 below summarizes the specifications for the optical payload.

Table 1: Summary of specifications

Specifications	***value***
focal length	$100\ mm$
Half FOV X	$2.20\ °$
Half FOV Y	$1.65\ °$
F#	1.5
Pixel size	$12\ \mu m$
Number of pixels	$640\ X\ \times\ 480\ Y$
Max X extent	$100\ mm$
Max Y extent	$250\ mm$
Max Z extent	$150\ mm$

3.2 Optical design

The system is designed with Zemax OpticStudio three freeform mirrors with a polynomial description. We used XY polynomials in the first place with null coefficients for the X and Y monomials, and used polynomials up to the 5^{th} order. As Zernike polynomials and XY polynomials describe the same subspace of surfaces (piston excluded) at any given order, it is possible to perform an analytical conversion from XY to Zernike. This allows to run additional optimisations using Fringe Zernike polynomials description. We allowed an optimisation up to the 5^{th} order with this basis as well. The stop was placed on the second mirror to achieve a more compact design.

The result is visible in Figure 1 below.

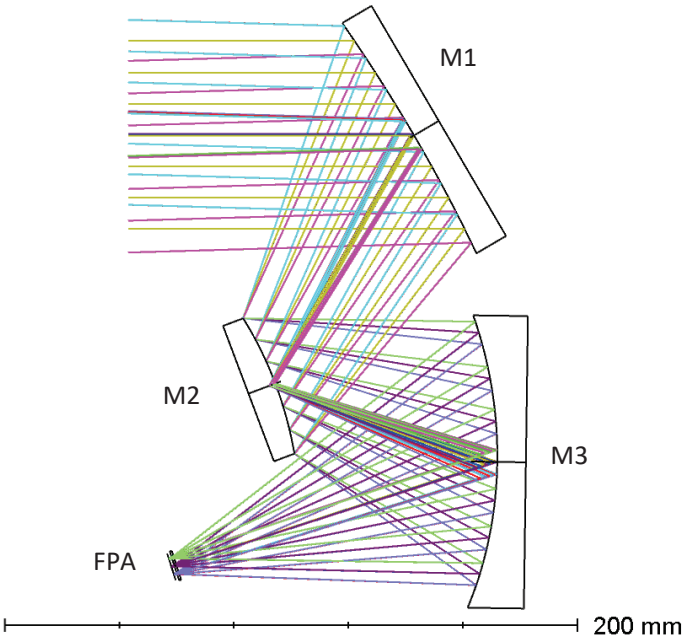

Figure 1: Optical system layout. FPA: Focal Plane Array

Figure 2 shows the RMS spot radius over the FOV and Figure 3 shows the polychromatic Modulation Transfer Function (MTF).

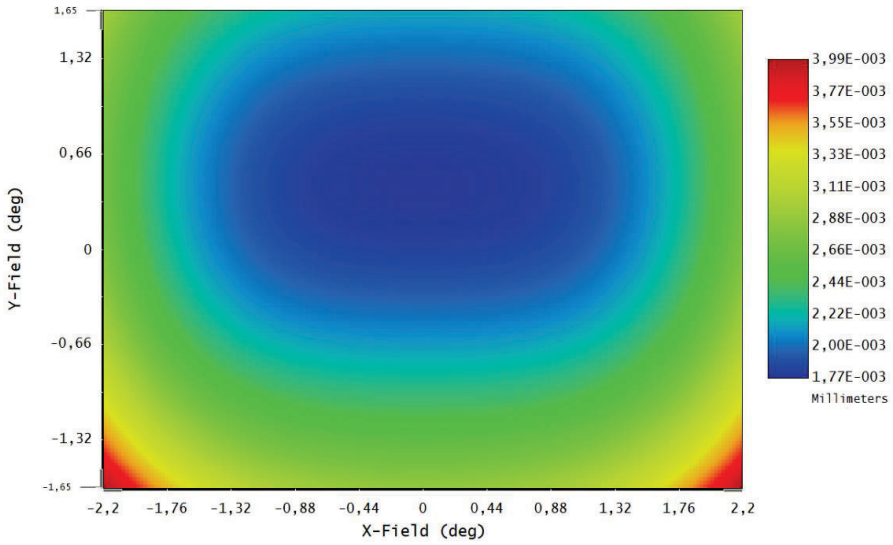

*Figure 2: RMS spot radius over the FOV. Airy radius =*18.3μm*, Min RMS spot radius =*1.77 μm*, Max RMS spot radius =*3.99μm

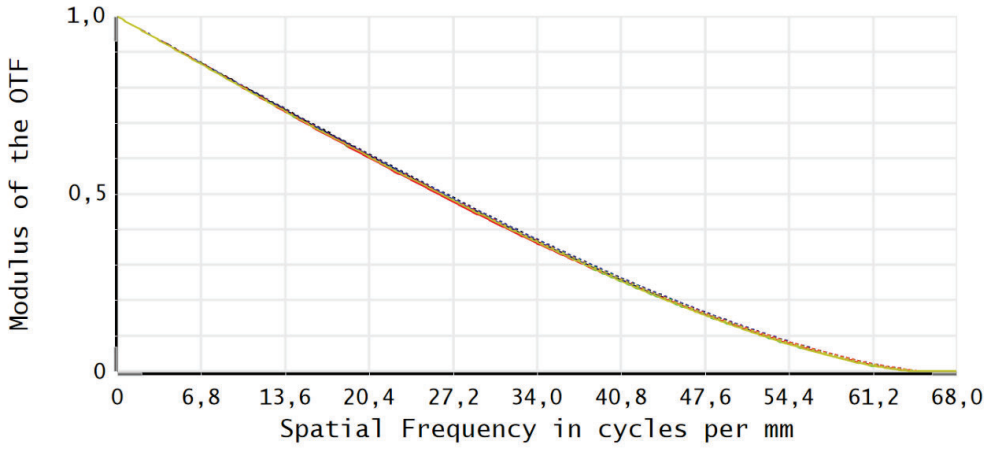

Figure 3: Modulation Transfer Function at 10 μm. The black lines show the diffraction limit in tangential (full line) and sagittal (dashed line) directions. On-axis field is represented by the blue lines, +X and +Y directions by the red and green lines and the top-right corner of the FoV is represented in yellow.

The system is diffraction limited for a 10 μm wavelength.

The tolerances to alignment have been calculated using a Monte Carlo algorithm with a thousand systems. The parameters used for the tolerancing analysis, as well as the results are given in Table 2 and 3:

Table 2: Tolerancing parameters

Parameter	***Value***
Mirror position	$100\ \mu m\ (X, Y)$
Mirror position	$50\ \mu m\ (Z)$
Mirror tilt	$0.03\ degrees\ (Rx, Ry)$
Mirror clocking	$0.1\ degree\ (Rz)$
Focal plane tilt	$0.1\ degree$

Table 3: Tolerancing results

Performances	
Nominal RMS spot radius (averaged on FOV)	$2.98\ \mu m$
Mean RMS spot radius	$3.95\ \mu m$
Standard deviation	$0.51\ \mu m$
Compensators	
M3 tilt about X standard deviation	$0.016\ degrees$
M3 tilt about Y standard deviation	$0.017\ degrees$
Focus standard deviation	$16\ \mu m$

These performances can be obtained by allowing adjusting the orientation of the third mirror in addition to the focal plane position. This enables to manufacture the system with large alignment tolerances.

4. ANALYSES AND MANUFACTURING

4.1 Mirrors sag & slope

To study the manufacturability of the mirrors, the departures from the best-fit spheres are plotted for each mirror, and given on figures 4, 5 and 6. The sagittal slopes are also given. The freeform departures of the mirrors do not exceed $650\ \mu m$, and can be manufactured[7]. In addition, the mirrors slopes are below $26\ mrad$, which is suitable for interferometric measurements.

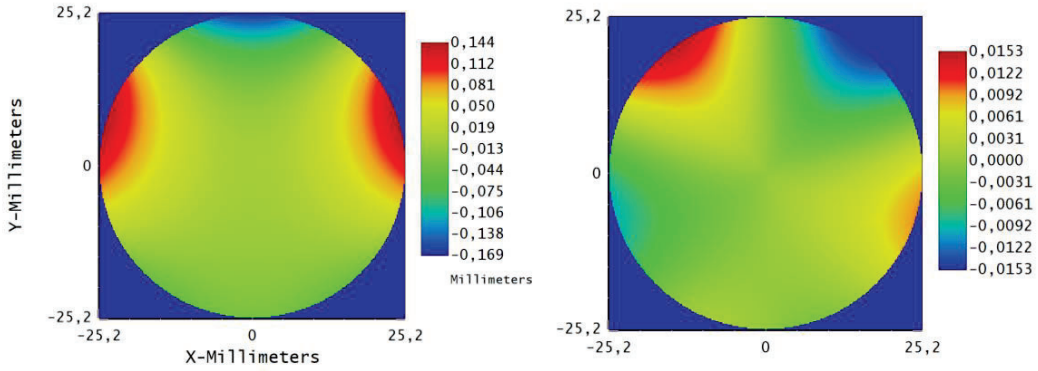

Figure 4: left: Freeform departure of M1 in mm – right: sagittal slope of M1 in radians

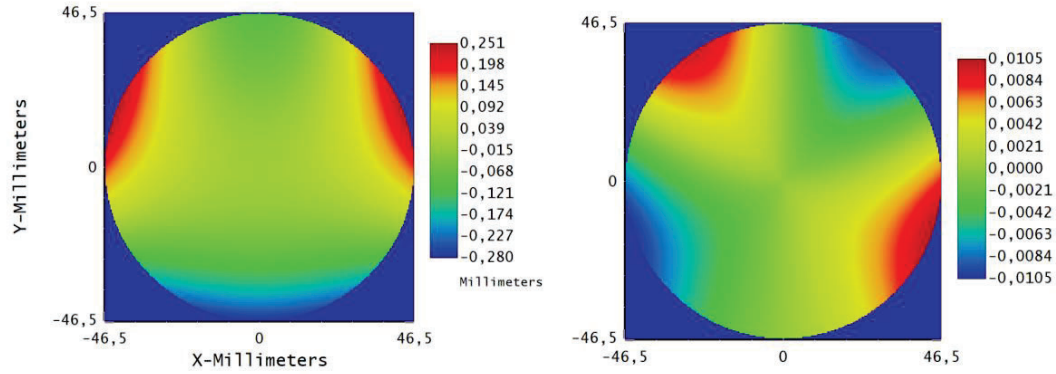

Figure 5: left: Freeform departure of M2 in mm – right: sagittal slope of M2 in radians

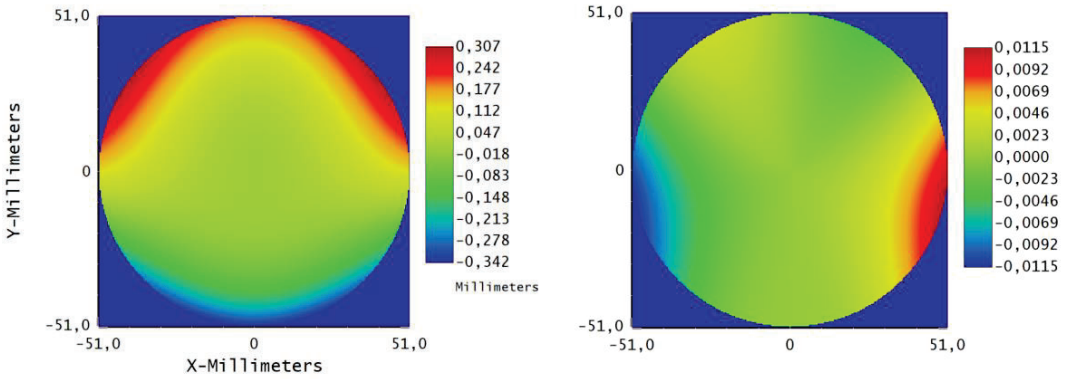

Figure 6: left: Freeform departure of M3 in mm – right: sagittal slope of M3 in radians

4.2 Mirror manufacturing & measurements

French optical manufacturing company Savimex manufactured the mirrors. They are made of Aluminium and shaped using Single Point Diamond Turning (SPDT). SPDT is a manufacturing technique for optical parts consisting in using a diamond-tipped cutting tool, and is use for high-quality aspheric or freeform optical components.

One of the main drawbacks of SPDT is the generation of Mid Spatial Frequency (MSF) errors due to the non-uniformity of the removal function of the instrument as it cuts through the material. These effects correspond to the movement of the tool head on the working piece, and can form circular patterns.

The form and slope errors from the mirrors specification, measured with LUPHOScan, a contactless metrology device, as well as residual RMS surface roughness are given in the table below:

Table 4: Form error, slope error and surface roughness of each mirror.

Mirror	*Form error – PV value [μm]*	*Slope error – maximum value [mrad]*	*RMS roughness [nm]*
M1	1.045	0.207	5.33
M2	1.096	0.212	6.23
M3	2.615	0.221	8.06

The mirrors can be seen on Figure 6. The blue layer is a protective cover that will be removed during the integration of the mirrors.

Figure 6: Mirrors of the TMA manufactured by SAVIMEX

4.3 System performances with real mirror data

In order to assess the effects of potential form error during the manufacturing of the mirrors and to verify that the requirements would still be met, the sag data retrieved from the LUPHOScan measurements were imported into the optical design software as grid sag surfaces.

The expected optical quality of the optical system taking into account the real mirror data is given below on figures 7 and 8. As can be seen, the system is no longer diffraction limited, with an average RMS spot radius of $20.5\ \mu m$ nor limited by the pixel size. In addition, the MTF shows severe degradation from the diffraction limit in both sagittal and tangential directions.

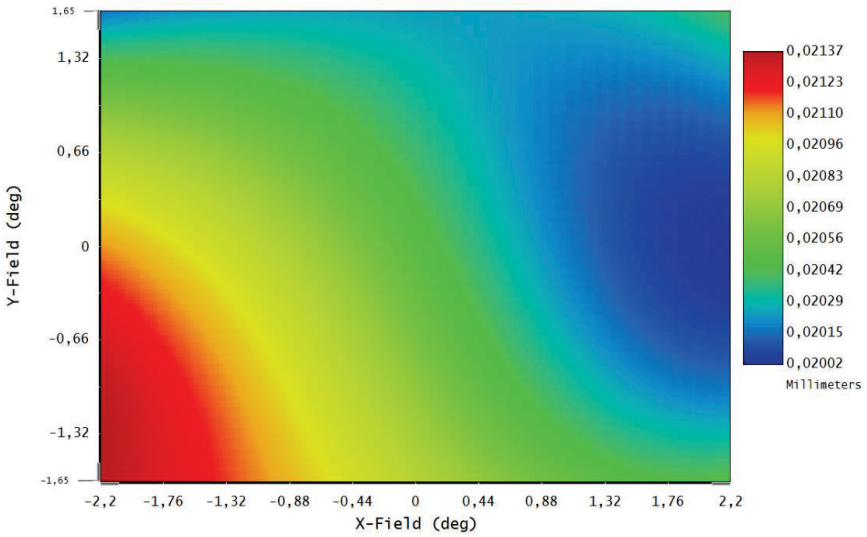

Figure 7: Simulated RMS spot radius over the FOV of the system with real mirror data. Airy spot radius =$18.3\ \mu m$*, Min RMS spot radius=*$20.02\ \mu m$*, Max RMS spot radius =*$21.37\mu m$

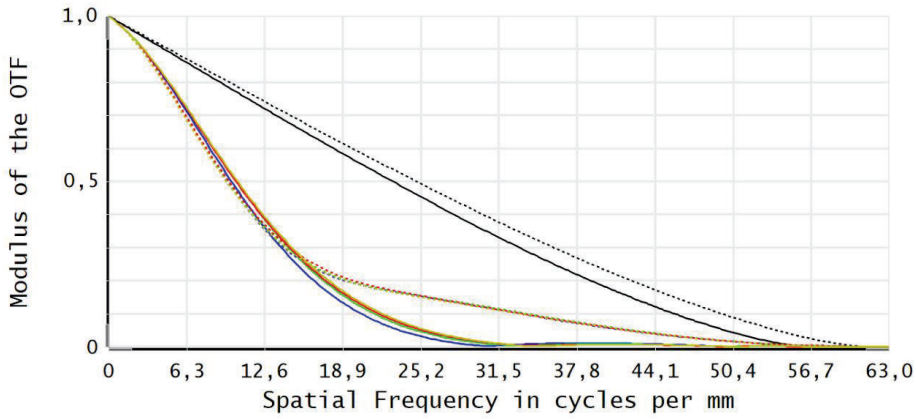

Figure 8: Simulated Modulation Transfer Function at 10 µm with real mirror data. The black lines show the diffraction limit in tangential (full line) and sagittal (dashed line) directions. On-axis field is represented by the blue lines, +X and +Y directions by the red and green lines and the top-right corner of the FoV is represented in yellow.

5. REOPTIMISATION AND RESULTS

In order to compensate for the loss in resolution induced by the mirrors form error, the system was re-optimized leaving as variables the mirrors position and orientation, while keeping the manufacturer data for the mirrors shape. The position of the FPA was also allowed to vary during the optimisation.

As a result, it was found that changes in the mirrors positions under $1\ mm$ compared to the original design, and changes in orientation in the order of a few tenth of a degree could result in a reduction of the RMS spot radius, down to an average radius of $7.63\ \mu m$. The corrected system is now close to the diffraction limit at $10\ \mu m$ over the major part of the FOV.

The simulated RMS spot radius size over the whole FOV of the corrected system and the FTM are shown on figures 9 and 10 below:

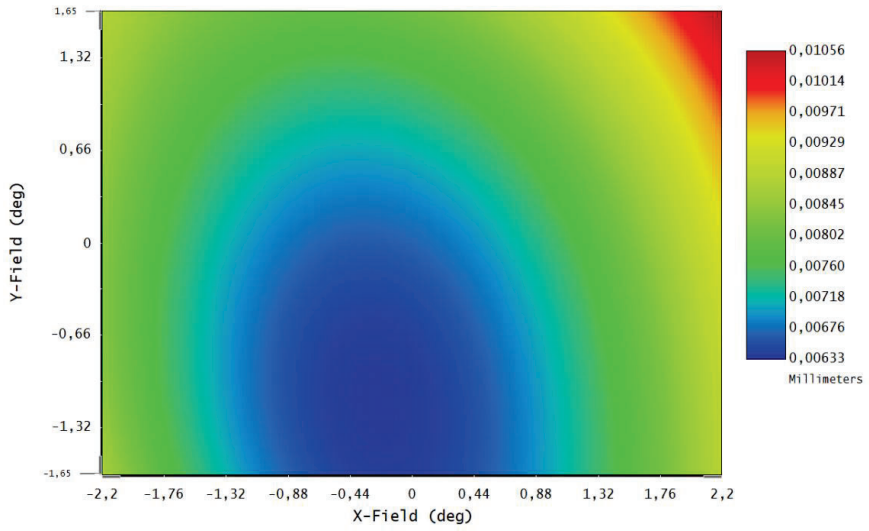

Figure 9: RMS spot radius over the FOV of the corrected system with real mirror data. Airy spot radius =18.3 µm, Min RMS spot radius=6.33 µm, Max RMS spot radius =10.56 µm

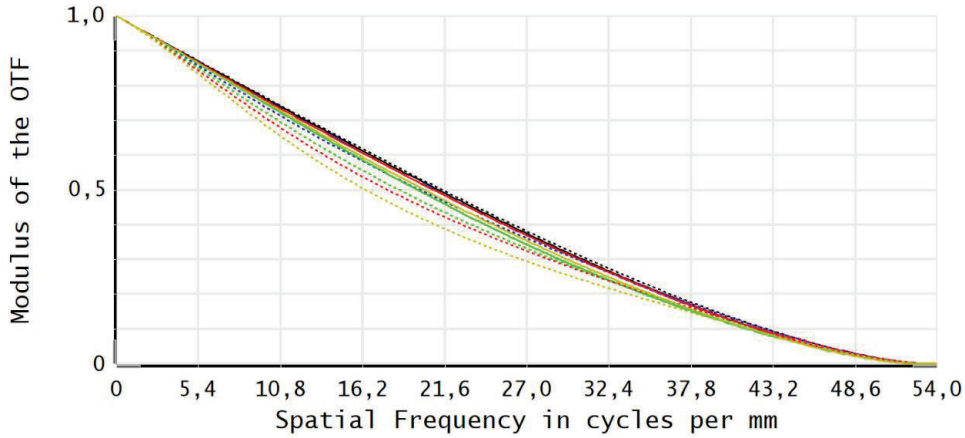

Figure 10: Simulated Modulation Transfer Function at 10 µm with the corrected system with real mirror data. The black lines show the diffraction limit in tangential (full line) and sagittal (dashed line) directions. On-axis field is represented by the blue lines, +X and +Y directions by the red and green lines and the top-right corner of the FoV is represented in yellow.

These corrections can be easily implemented in the optomechanical design, which has been manufactured by French company Optique Microsystèmes, who is also in charge of the integration of the whole instrument, which is shown on Figure 11.

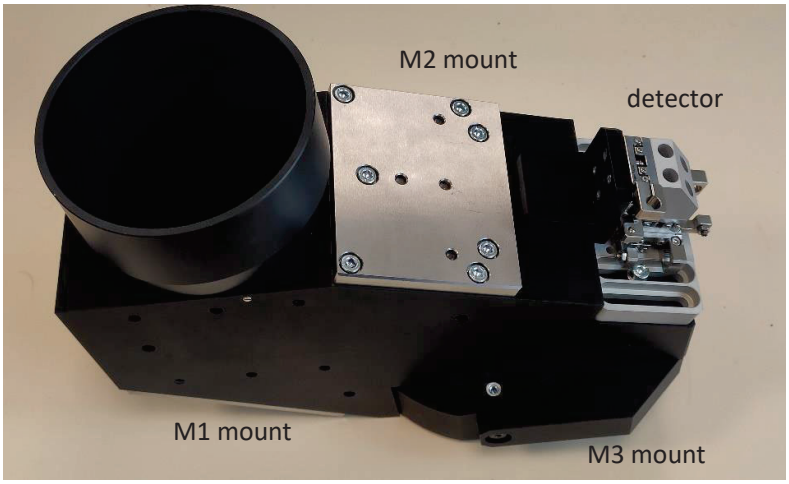

Figure11: Full system. Mechanical housing and integration by Optique Microsystèmes

6. CONCLUSION

In this article, we presented a proof of concept for an infrared thermal imaging payload for a 12U nanosatellite suited for applications such as Urban Heat Islands temperature monitoring. The design is based on an unobscured, high aperture, freeform TMA using an uncooled micro bolometer. The performances of the system are compliant with the specifications and require minimal alignment. Furthermore, measurements of the mirrors' shape errors were performed, and the system was re-optimised using the manufacturer's data to compensate for the loss in image quality induced by the shape errors in the manufacturing of the mirrors. A straylight analysis, not presented in this paper, was also performed, and an adequate baffling to prevent specular out of field straylight was added[8].

As the system is in its integration phase at the time of writing, experimental characterisation of the instrument will not be presented.

ACKNOWLEDGEMENTS

The authors are thankful for the funding support from the European Space Agency (ESA), as well as Savimex for the mirrors manufacturing and LUPHOSCAN measurements and Optique Microsystèmes for the optomechanical design.

REFERENCES

[1] Santamouris, M., "Regulating the damaged thermostat of the cities | Status, impacts and mitigation challenges," Energy and Buildings 91, 43{56 (Mar. 2015).

[2] Fang, F. Z., Zhang, X. D., Weckenmann, A., Zhang, G. X., & Evans, C. (2013). "Manufacturing and measurement of freeform optics". CIRP Annals, 62(2), 823-846.

[3] Eric M. Schiesser, Aaron Bauer, and Jannick P. Rolland, "Effect of freeform surfaces on the volume and performance of unobscured three mirror imagers in comparison with off-axis rotationally symmetric polynomials," Opt. Express **27**, 21750-21765 (2019)

[3] Fuerschbach, K., Rolland, J. P., and Thompson, K. P., "A new family of optical systems employing φ-polynomial surfaces," Optics Express 19, 21919 (Oct. 2011).

[4] Cakmakci, O., Vo, S., Foroosh, H., and Rolland, J., "Application of radial basis functions to shape description in a dual-element off-axis magnifier," Optics Letters 33, 1237 (June 2008).

[5] Gross, H., Brömel, A., Beier, M., Steinkopf, R., Hartung, J., Zhong, Y., Oleszko, M., and Ochse, D.,"Overview on surface representations for freeform surfaces," 96260U (Sept. 2015).

[6] Druart, G., Allioux, R., Perrault, P., Lefranc, V., Cariou, N., and Rousset-Rouvière, L., "Study of Infrared optical payloads to be integrated in a nanosat," in [Optical Design and Engineering VII], Mazuray, L., Wartmann, R., and Wood, A. P., eds., 18, SPIE, Frankfurt, Germany (June 2018).

[7] Matthias Beier, Johannes Hartung, Thomas Peschel, Christoph Damm, Andreas Gebhardt, Sebastian Scheiding, Daniela Stumpf, Uwe D. Zeitner, Stefan Risse, Ramona Eberhardt, and Andreas Tünnermann, "Development, fabrication, and testing of an anamorphic imaging snap-together freeform telescope," Appl. Opt. 54, 3530-3542 (2015)